Carbon Materials

DOI: 10.1002/anie.201408856

Nanoporous Carbon Tubes from Fullerene Crystals as the π-Electron Carbon Source**

Lok Kumar Shrestha, Rekha Goswami Shrestha, Yusuke Yamauchi,* Jonathan P. Hill, Toshiyuki Nishimura, Kun'ichi Miyazawa, Takazumi Kawai, Susumu Okada, Katsunori Wakabayashi, and Katsuhiko Ariga**

Abstract: *Here we report the thermal conversion of one-dimensional (1D) fullerene (C_{60}) single-crystal nanorods and nanotubes to nanoporous carbon materials with retention of the initial 1D morphology. The 1D C_{60} crystals are heated directly at very high temperature (up to 2000°C) in vacuum, yielding a new family of nanoporous carbons having π-electron conjugation within the sp^2-carbon robust frameworks. These new nanoporous carbon materials show excellent electrochemical capacitance and superior sensing properties for aromatic compounds compared to commercial activated carbons.*

Fullerenes,[1] carbon nanotubes,[2] and graphenes[3] have well-defined molecular surfaces almost entirely composed of sp^2-carbon atoms, which provide extended conjugated π-systems to realize their intriguing optoelectronic properties. Recently, self-assembled fullerene (C_{60}) nanostructures have received considerable attention due to their unique physicochemical properties and high symmetries with conjugated π-systems. Many potential applications have been demonstrated in a wide range of research fields, including biomedicines, semiconductors, and optoelectric/spintronic devices.[4] Introduction of nanoporous architectures into sp^2-carbon materials is anticipated to drastically increase the effective surface area leading to great utility in many applications such as high-power solar cells, supercapacitors, hydrogen storage materials, and high sensitivity chemical and physical sensors.[5]

Due to their low costs, high chemical and mechanical stabilities, and high conductivities as well as high surface areas and extensive pore structures, nanoporous (mesoporous) carbon materials have been extensively used in different applications, including as catalyst supports, adsorbents, and sensors.[6] The hard-templating approach is well known as a powerful tool for the preparation of nanoporous carbons.[7] Inorganic mesoporous silicas and zeolites have often been utilized as templates. Polyvinyl chloride, polypyrrol, furfuryl alcohol, sucrose, acenaphthene, and mesophase pitch have been utilized as carbon sources. However, such carbon sources cannot be easily graphitized in the pore walls without catalysts such as Fe and Co.[6,7] There are also recent reports of alternative approaches demonstrating direct self-assembly of amphiphilic molecules as a soft template for nanoporous carbons.[8] In particular, the formation of highly graphitic walls having extended conjugated π-systems in nanoporous carbons still remains a challenging task and would lead to several benefits. Apart from expected improvements in electrical conductivity, the introduction of highly graphitized walls should promote the stability of the carbon support, thus improving its durability.

Inspired by the above situation, in this work we aimed at synthesizing a new family of carbon materials by utilizing single-crystal C_{60} assemblies as ideal π-electron carbon sources, because C_{60} consists essentially of a π-electron system (similar to graphite, which is composed of stacked graphene sheets of linked 'hexagonal' rings). In this Commu-

[*] Dr. L. K. Shrestha, Prof. Y. Yamauchi, Dr. J. P. Hill, Dr. K. Wakabayashi, Prof. K. Ariga
World Premier International Center for Mater Nanoarchitectonics (WPI-MANA), National Institute for Materials Science (NIMS)
1-1 Namaiki, Tsukuba, Ibaraki 305-0044 (Japan)
E-mail: SHRESHTA.Lokkumar@nims.go.jp
YAMAUCHI.Yusuke@nims.go.jp
ARIGA.Katsuhiko@nims.go.jp

Dr. R. G. Shrestha
Department of Pure and Applied Chemistry, Faculty of Science and Technology, Tokyo University of Science
2641 Yamazaki, Noda, Chiba 278-8510 (Japan)

Dr. T. Nishimura
Sialon Unit, Environment and Energy Materials Division
National Institute for Materials Science (NIMS)
1-1 Namaiki, Ibaraki, Tsukuba 305-0044 (Japan)

Prof. K. Miyazawa
Materials Processing Unit, Advanced Key Technologies Division
National Institute for Materials Science (NIMS)
1-1 Namaiki, Ibaraki, Tsukuba 305-0044 (Japan)

Prof. T. Kawai
Knowledge Discovery Research Laboratories, NEC Corporation
1753 Shimonumabe, Nakahara-ku, Kawasaki Kanagawa 211-8666 (Japan)

Prof. S. Okada
Graduate School of Pure and Applied Sciences, University of Tsukuba, Tsukuba, Ibaraki 305-8571 (Japan)

[**] This research was partially supported by the Grant-in-Aid for Young Scientists A (26708028) and B (25790021) of the Japan Society for the Promotion of Science (JSPS), the Japan-Taiwan Cooperative Program of the Japan Science and Technology Agency (JST), and The Canon Foundation.

Supporting information for this article (including detailed experimental procedures, additional SEM and TEM images, additional results obtained from thermogravimetric analysis, cyclic voltammetry, and X-ray photoelectron spectroscopy, and results obtained from theoretical calculations) is available on the WWW under http://dx.doi.org/10.1002/anie.201408856.

nication, we report a novel pathway for the synthesis of nanoporous carbons with graphitic walls by heat treatment (2000 °C in vacuum) of 1D C_{60} nanorods (FNR) and C_{60} nanotubes (FNT).

For the preparation of 1D FNR and FNT, we used a liquid–liquid interfacial precipitation (LLIP) method, which is one of the most promising methods for preparing C_{60} crystals.[9] The 1D FNR was prepared at the interface between *tert*-butyl alcohol (TBA) and a saturated solution of C_{60} in mesitylene (0.99 mg mL^{-1}), whereas 1D FNT was prepared at the interface between isopropyl alcohol (IPA) and a saturated solution of C_{60} in mesitylene. For FNR, the TBA solution was slowly added to a saturated C_{60} solution in mesitylene. The mixture was stored in a temperature-controlled incubator at 25 °C for 24 h. Similarly, FNT was grown with IPA as antisolvent. Detailed synthetic methods are supplied in the Supporting Information (SI).

As shown in Figure S1, FNR prepared using the TBA system consist of straight rods. Based on a histogram obtained by measuring 100 randomly selected FNR, rod lengths are in the range from 7–40 μm (Figure S2 a). Rod diameters are found typically in the range from 250 nm to 1.2 μm, with a small fraction of rods having diameters greater than 1.2 μm (Figure S2 b). FNT prepared using the IPA system consist of hollow cavities at both ends of the straight rods (the cavities are not connected, that is, FNT are only locally tubular in morphology). Scanning electron microscopy (SEM) and transmission electron microscopy (TEM) images of FNT supplied in Figure S3 show typical tubular structure.[10] Their lengths and diameters are in the range of approximately 7–40 μm (Figure S4 a) and 300 nm to 1.2 μm (Figure S4 b), respectively. SEM and TEM images show that individual FNR and FNT possess very smooth surfaces along their entire lengths. Lattice fringes in high-resolution TEM (HR-TEM) images show that both FNR and FNT are composed of individual C_{60} single crystals. The FNT formation in the IPA system is considered due to the well-known core dissolution mechanism. In solution, FNR are solvated in the initial state and the surface of the solvated rods is insoluble in the solvent during their growth. The cores of the solvated rods are redissolved in the solution, forming the tubular structure. Careful observation of SEM images (Figure S1 a) shows that the edges of FNR are partially dissolved forming a cone type structure, indicating that the solid solvates obtained from the IPA/mesitylene system are more stable than those obtained from the TBA/mesitylene system.

The precursors (FNR and FNT) were heated at 2000 °C in vacuum to obtain nanoporous carbons, which are hereafter abbreviated as HT-FNR and HT-FNT, respectively. Figures 1 and S5 show SEM and TEM images of HT-FNT and HT-FNR. Although the original 1D morphology of FNR and FNT remains essentially unchanged after heat treatment, most of the rod structures have some distortion by slight bending, although the uniform diameters of rods or tubes is maintained (Figures S6 and S7). High-resolution SEM images confirm clearly that nanopores are approximately 40–50 nm in size and that they are randomly distributed on the surface of the samples (Figures S6 and S7). Similar results are obtained by TEM measurements (Figures S8 and S9). Nitrogen adsorption–desorption isotherms (Figure S10) show that the nitrogen uptakes of HT-FNR and HT-FNT are drastically increased in the high-pressure range over the FNT precursor, indicating the formation of large-sized pores. The Brunauer–Emmett–Teller (BET) surface area of HT-FNR is around 1600 m^2 g^{-1}, whereas that of HT-FNT is around 1650 m^2 g^{-1}. These values are comparable to commercially available activated carbons (1000–1500 m^2 g^{-1}), mesoporous carbons (500–1000 m^2 g^{-1}), and carbon nanotubes (1300 m^2 g^{-1} for single-walled carbon nanotubes).[11] In addition to the significant enhancement in surface area, heat treatment causes a microstructural transformation of C_{60} single crystals into randomly oriented graphitic carbon.[12] Careful examination of HR-TEM images indicate that a maximum stacking of six graphene layers with a ca. 0.35 nm interlayer spacing is observed for HT-FNR (Figures S5 and S11) and HT-FNT (Figures 1 b and S12).

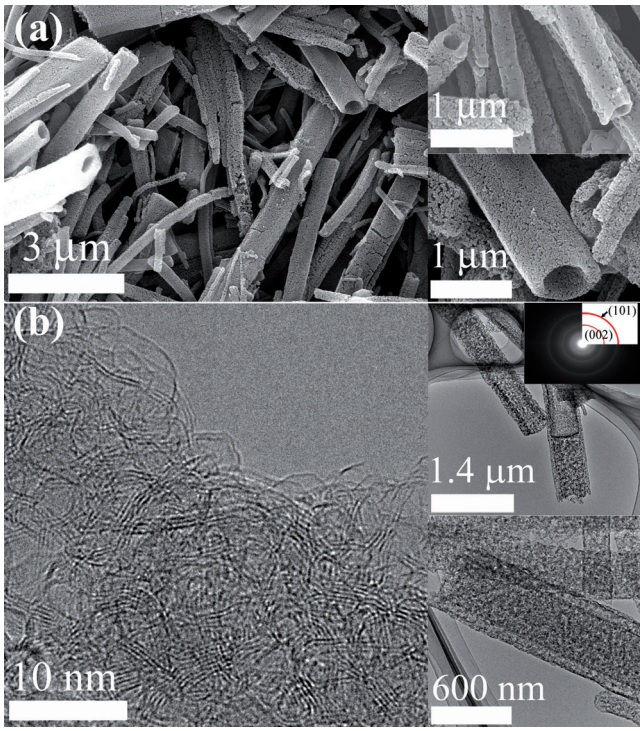

Figure 1. Electron microscopic observation of 1D nanoporous carbon tubes prepared by thermal conversion of FNT. (a) SEM images and (b) HR-TEM and TEM images. High magnification TEM image reveals the highly graphitic form of the nanoporous structure.

The direct conversion of C_{60} single-crystal nanotubes to high-surface-area nanoporous carbon tubes with graphitic walls has not been well explored. To understand the structural evolution of the pore walls, theoretical calculations were performed. We employed tight-binding molecular dynamics (TBMD) simulations for C_{60} crystals at finite temperatures under a constant pressure. The starting point was a face-centered cubic (fcc) structure containing four C_{60} molecules in the unit cell. The temperature was fixed at 4000 K, and the pressure fixed at 10 GPa. Although the temperature and pressure were set higher than the actual experimental conditions (to accelerate the structural evolution and reduce

the time required for computation), the parameter set is considered to reflect well the qualitative behavior of thermal structural evolution. Computational results show that interfullerene bonds are formed and broken frequently at high temperature and pressure. Under these conditions, carbon atoms mostly take up three-coordinate structures, and interfullerene bonds are favored, because the formation of those bonds reduces the curvature of the initial fullerenes. Subsequently, interfullerene bonds gradually become dominant in the direction of the nearest neighbor fullerene. Figure S13 shows the structure of heat-treated C_{60} crystal after 25.5 ps. It can be clearly seen that a graphite-like layered structure has developed. In addition, the carbon atoms are bonded in a hexagonal honeycomb structure within each plane. Thus, simulation data strongly supports the conversion of 0D fullerene C_{60} into a 2D graphitic structure (Movie S1, and Figures S13–S15). This C_{60}-derived nanoporous carbon shows extremely high thermal stability without any loss of surface area (Figure S16).[13]

To further investigate the abovementioned structural evolution, wide-angle XRD patterns and Raman scattering spectra were measured for FNR and FNT crystals before and after heat treatment. As shown in Figure 2a, in contrast to

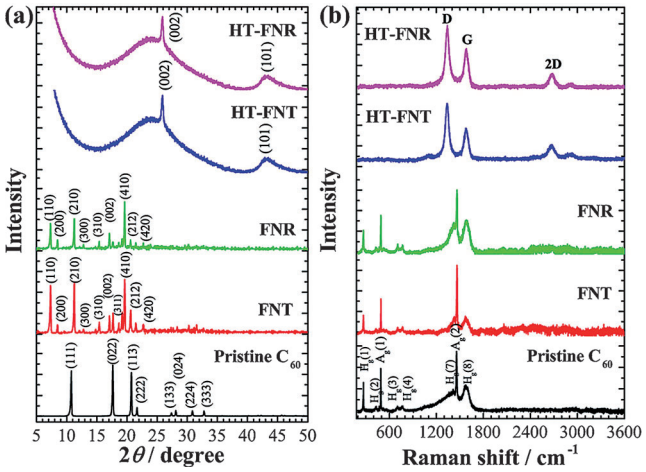

Figure 2. (a) Wide-angle XRD patterns and (b) Raman scattering spectra of FNR and FNT before and after heat treatment. Wide-angle XRD patterns of FNR and FNT are indexed to the hcp structure.

pristine C_{60}, which possesses the fcc crystal structure, FNR and FNT synthesized here have hexagonal close-packed (hcp) crystal structures. The lattice parameters of the hcp crystals were $a = 2.402$ nm, $c = 1.305$ nm for FNR, and $a = 2.403$ nm, $c = 1.305$ nm for FNT. The hcp crystal structure of C_{60} has often been observed in C_{60} crystals grown by LLIP or slow evaporation methods, due to the entrapment of solvent molecules during crystallization.[14] After heat treatment, diffraction peaks due to FNR and FNT crystals disappear with a single sharp diffraction peak emerging at $2\theta \approx 26°$. This peak can be indexed to the (002) plane (i.e., interlayer spacing) of a graphitic structure. For these samples, the d spacing (0.3441 nm) is very close to that estimated from HR-TEM images, but slightly larger than that of bulk graphite (0.3345 nm). This is due to the turbostatic nature of graphene sheets, as shown in Figure 1b. The broad diffraction peak at approximately 42° can be indexed to the (101) graphite plane, confirming the presence of weak intralayer-ordering of the graphene layers in HT-FNR and HT-FNT samples.

As shown in Figure 2b, Raman spectra of FNR and FNT correspond to that of pristine C_{60}, containing eight vibration bands: two A_g and six H_g bands. Raman bands of pristine C_{60} at 495.5 and 1464 cm^{-1} correspond to the breathing $A_g(1)$ mode and the pentagonal pinch $A_g(2)$ mode of the C_{60} molecule. The other bands correspond to $H_g(1)$, $H_g(2)$, $H_g(3)$, $H_g(4)$, $H_g(7)$, and $H_g(8)$ vibration modes.[15] In HT-FNR and HT-FNT samples, all Raman bands due to pristine C_{60} disappear and new bands appear at ca. 1335 and 1582 cm^{-1}. Additionally, a clear Raman band at 2672 cm^{-1} also appears. These bands correspond to D, G, and 2D bands of carbon, respectively.[16] The D band (defect-induced) corresponds to the presence of disordered carbon, whereas the G band represents a graphitic structure corresponding to the stretching vibration mode. Appearance of a sharp D band with a clear 2D band is a strong evidence for the formation of crystalline carbon materials, as shown in Figures S11 and S12. Thus, the Raman data presented in Figure 2b give a clear indication of the conversion of crystalline fullerenes to graphitic structures.

The chemical states of elements in FNR, FNT, HT-FNR, and HT-FNT were characterized by X-ray photoelectron spectroscopy (XPS). XPS survey spectra of pristine C_{60}, FNT, FNR, HT-FNT, and HT-FNR (Figure S17a) display the presence of C1s and O1s core level peaks. Careful examination of the XPS spectra shows that the relative peak intensity of the O1s core level of HT-FNT and HT-FNR samples is lower compared to the pristine C_{60}, FNT, and FNR, demonstrating the removal of oxygen-containing functional groups by heat treatment. Figure S17b shows a deconvolution of the C1s peak of HT-FNT. The four deconvoluted peaks of HT-FNT at 284.6, 286.2, 286.8, and 287.4 eV correspond to C=C (sp^2 carbon), C–C (sp^3 carbon), C–O, and C=O, respectively. Compared to FNT, the oxygen-containing functional groups (C–O and C=O) are decreased in HT-FNT. The XPS O 1s spectra of FNT and HT-FNT are shown in Figure S18.

For HT-FNT and HT-FNR samples, we measured cyclic voltammetry (CV) curves in 1M H_2SO_4 in the potential range from 0 to 1 V (vs. Ag/AgCl) using different scan rates of 5–100 mV s^{-1} (Figures 3a and S19). The CV curves obtained show a very rapid current response and exhibit roughly rectangular profiles, features that are reminiscent of electrical double layer capacitors. In fact, a rectangular CV profile is the ideal state for supercapacitor applications. In general, with increasing scan rates, the electrolyte diffusion in porous systems is obstructed, so that the CV profile departs from an ideal rectangular shape. However, the CV profiles of HT-FNT and HT-FNR samples demonstrate fast electrolyte diffusion and high capacitance at high scan rates, due to an increase in the electrochemically accessible surface area. Specific capacitances are 145.5 F g^{-1} (for HT-FNT) and 132.3 F g^{-1} (for HT-FNR) at a scan rate of 5 mV s^{-1} (Figure 3b). The presence of hollow cavities in HT-FNT improves the accessibility of guest molecules from the exterior even under high scan rates, preventing any serious loss in capacitance (Figure 3b).

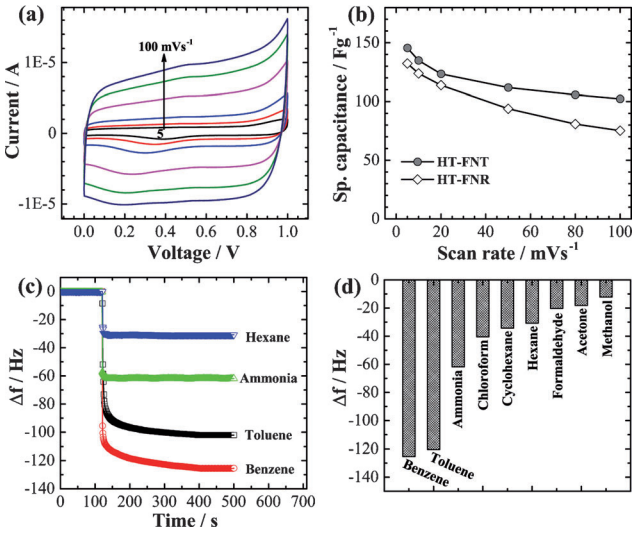

Figure 3. (a) CV curves of HT-FNT at different scan rates (5, 10, 20, 50, 80, and 100 mVs^{-1}), (b) specific capacitance vs. scan rates for HT-FNR and HT-FNT, (c) QCM frequency shifts (Δf) upon exposure of hexane, ammonia, benzene, and toluene, and (d) summary of frequency shifts (Δf) of HT-FNT QCM electrode upon exposure of various gaseous molecules.

Recently, molecular sensing of toxic organic substances has gained importance and is investigated extensively. Experiments have shown that a well-designed host architecture (especially high surface area and high pore volume of materials) is required for effective sensing. Therefore, we determined the vapor-sensing capacities of our materials for toxic aromatic solvents using the quartz crystal microbalance (QCM) technique. Figure 3c shows the time dependence of frequency shifts (Δf) for a QCM electrode prepared using the HT-FNT sample after exposure to different solvent vapors as typical example. Figure 3d shows the summary of frequency shifts (Δf) of the HT-FNT QCM electrode after exposure to various gaseous molecules. Sensing of solvent vapors could be repetitively performed by alternate exposure and removal of solvent molecules (Figure S20). Frequency shifts are rapid (only a few seconds) upon exposure of the sensor to solvent molecules. The adsorption of aromatic solvent vapors such as benzene (125 Hz) and toluene (120 Hz) lead to much larger frequency shifts than for aliphatic solvent vapors, including cyclohexane (34 Hz) and hexane (30 Hz). Sensing capacities of aromatic solvents are roughly three times greater than for aliphatic hydrocarbons of almost similar molecular size and weight. This result demonstrates that our nanoporous carbon tubes derived from C_{60} crystals exhibit excellent sensitivity and selectivity toward aromatic solvent molecules. This is due to easy and free diffusion of aromatic solvent vapors into the nanopores utilizing π–π interaction between solvent molecules and sp^2-bonded graphitic carbon frameworks.[17]

To conclude, we have succeeded in preparing a new type of nanoporous carbon material with graphitized frameworks through the optimized thermal conversion of high purity C_{60} single crystals. We strongly believe that our synthetic concept represents a new avenue for the preparation of multifunctional carbon nanomaterials, which are not attainable by traditional approaches to prepare mesoporous/nanoporous carbons.[7,8]

Received: September 5, 2014
Revised: October 16, 2014
Published online: November 25, 2014

Keywords: carbon nanotubes · fullerene crystals · graphene · nanoporous carbon · π-conjugated system

[1] H. W. Kroto, J. R. Heath, S. C. O'Brien, R. F. Curl, R. E. Smalley, *Nature* **1985**, *318*, 162–163.
[2] S. Lijima, *Nature* **1991**, *354*, 56–58.
[3] a) K. S. Novoselov, A. K. Geim, S. V. Morozov, D. Jiang, Y. Zhang, S. V. Dubonos, I. V. Grigorieva, A. A. Firsov, *Science* **2004**, *306*, 666–669; b) L. Liu, Z. Niu, L. Zhang, W. Zhou, X. Chen, S. Xie, *Adv. Mater.* **2014**, *26*, 4855–4862; c) Z. Niu, L. Liu, L. Zhang, Q. Shao, W. Zhou, X. Chen, S. Xie, *Adv. Mater.* **2014**, *26*, 3681–3687; d) Z. Niu, L. Zhang, L. Liu, B. Zhu, H. Dong, X. Chen, *Adv. Mater.* **2013**, *25*, 4035–4042.
[4] a) R. C. Haddon, L. E. Brus, K. Raghavachari, *Chem. Phys. Lett.* **1986**, *125*, 459–464; b) S. Zhou, C. Burger, B. Chu, M. Sawamuraa, N. Nagahama, M. Toganoh, U. E. Hackler, H. Isobe, E. Nakamura, *Science* **2001**, *291*, 1944–1947; c) S.-I. Kobayashi, S. Mori, S. Iida, H. Ando, T. Takenobu, Y. Taguchi, A. Fujiwara, A. Taninaka, H. Shinohara, Y. Iwasa, *J. Am. Chem. Soc.* **2003**, *125*, 8116–8117; d) K. Komatsu, M. Murata, Y. Murata, *Science* **2005**, *307*, 238–240; e) J. L. Segura, N. Martín, D. M. Guldi, *Chem. Soc. Rev.* **2005**, *34*, 31–47; f) T. Homma, K. Harano, H. Isobe, E. Nakamura, *Angew. Chem. Int. Ed.* **2010**, *49*, 1665–1668; *Angew. Chem.* **2010**, *122*, 1709–1712; g) M. Gobbi, F. Golmar, R. Llopis, F. Casanova, L. E. Hueso, *Adv. Mater.* **2011**, *23*, 1609–1613; h) X. Zhang, S. Mizukami, T. Kubota, Q. Ma, M. Oogane, H. Naganuma, Y. Ando, T. Miyazaki, *Nat. Commun.* **2013**, *4*, 1392–1–7; i) R. Saran, V. Stolojan, R. J. Curry, *Sci. Rep.* **2014**, *4*, 5041–5049; j) M. J. Hollamby, M. Karny, P. H. H. Bomans, N. A. J. M. Sommerdjik, A. Saeki, S. Seki, H. Minamikawa, I. Grillo, B. R. Pauw, P. Brown, J. Eastoe, H. Möhwald, T. Nakanishi, *Nat. Chem.* **2014**, *6*, 690–696; k) W. Nakanishi, K. Minami, L. K. Shrestha, Q. Ji, J. P. Hill, K. Ariga, *Nano Today* **2014**, *9*, 378–394.
[5] a) M. Sathish, K. Miyazawa, T. Sasaki, *Chem. Mater.* **2007**, *19*, 2398–2400; b) L. K. Shrestha, Y. Yamauchi, J. P. Hill, K. Miyazawa, K. Ariga, *J. Am. Chem. Soc.* **2013**, *135*, 586–589; c) L. K. Shrestha, Q. Ji, T. Mori, K. Miyazawa, Y. Yamauchi, J. P. Hill, K. Ariga, *Chem. Asian J.* **2013**, *8*, 1662–1679.
[6] a) K. Ariga, A. Vinu, Y. Yamauchi, Q. Ji, J. P. Hill, *Bull. Chem. Soc. Jpn.* **2012**, *85*, 1–32; b) P. Su, L. Jiang, J. Zhao, J. Yan, C. Li, Q. Yang, *Chem. Commun.* **2012**, *48*, 8769–8771; c) J. Tang, J. Liu, N. L. Torad, T. Kimura, Y. Yamauchi, *Nano Today* **2014**, *9*, 305–323.
[7] a) J. Lee, S. Yoon, T. Hyeon, S. M. Oh, K. B. Kim, *Chem. Commun.* **1999**, 2177–2178; b) S. Han, K. Sohn, T. Hyeon, *Chem. Mater.* **2000**, *12*, 3337–3341; c) T. Kyotani, T. Nagai, S. Inoue, A. Tomita, *Chem. Mater.* **1997**, *9*, 609–615; d) Z. X. Ma, T. Kyotani, A. Tomita, *Chem. Commun.* **2000**, 2365–2366; e) K. P. Gierszal, M. Jaroniec, T. W. Kim, J. Kim, R. Ryoo, *New J. Chem.* **2008**, *32*, 981–993; f) A. B. Fuertes, T. A. Centeno, *J. Mater. Chem.* **2005**, *15*, 1079–1083; g) A. B. Fuertes, S. Alvarez, *Carbon* **2004**, *42*, 3049–3055.
[8] a) Y. Meng, D. Gu, F. Q. Zhang, Y. F. Shi, H. F. Yang, Z. Li, C. Z. Yu, B. Tu, D. Y. Zhao, *Angew. Chem. Int. Ed.* **2005**, *44*, 7053–7059; *Angew. Chem.* **2005**, *117*, 7215–7221; b) F. Q. Zhang, Y. Meng, D. Gu, Y. Yan, C. Z. Yu, B. Tu, D. Y. Zhao, *J. Am. Chem. Soc.* **2005**, *127*, 13508–13509; c) J. Liu, T. Y. Yang, D. W. Wang,

G. Q. Lu, D. Y. Zhao, S. Z. Qiao, *Nat. Commun.* **2013**, *4*, 2798 – 2797.

[9] a) K. Miyazawa, Y. Kuwasaki, A. Obayashi, M. Kuwabara, *J. Mater. Res.* **2002**, *17*, 83 – 88; b) K. Miyazawa, *J. Am. Ceram. Soc.* **2002**, *85*, 1297 – 1299; c) M. Sathish, K. Miyazawa, J. P. Hill, K. Ariga, *J. Am. Chem. Soc.* **2009**, *131*, 6372 – 6373; d) J. Jeong, W. S. Kim, S. I. Park, T. S. Yoon, B. H. Chung, *J. Phys. Chem. C* **2010**, *114*, 12976 – 12981; e) L. K. Shrestha, J. P. Hill, T. Tsuruoka, K. Miyazawa, K. Ariga, *Langmuir* **2013**, *29*, 7195 – 7202; f) L. K. Shrestha, M. Sathish, J. P. Hill, K. Miyazawa, T. Tsuruoka, N. Sanchez-Ballester, I. Honma, Q. Ji, K. Ariga, *J. Mater. Chem. C* **2013**, *1*, 1174 – 1181.

[10] a) E. Abdullayev, Y. Lvov, *J. Mater. Chem.* **2010**, *20*, 6681 – 6687; b) D. Fix, D. Andreeva, H. Möhwald, Y. Lvov, D. Shchukin, *Adv. Funct. Mater.* **2009**, *19*, 780 – 786.

[11] a) C. Liang, Z. Li, S. Dai, *Angew. Chem. Int. Ed.* **2008**, *47*, 3696 – 3717; *Angew. Chem.* **2008**, *120*, 3754 – 3776; b) Y. Zhu, S. Murali, M. D. Stoller, K. J. Ganesh, W. Cai, P. J. Ferreira, Aa. Pirkle, R. M. Wallace, K. A. Cychosz, M. Thommes, D. Su, E. A. Stach, R. S. Ruoff, *Science* **2011**, *332*, 1537 – 1541; c) M. Hu, J. Reboul, S. Furukawa, N. L. Torad, Q. Ji, P. Srinivasu, K. Ariga, S. Kitagawa, Y. Yamauchi, *J. Am. Chem. Soc.* **2012**, *134*, 2864 – 2867.

[12] a) K. Asaka, T. Nakayama, K. Miyazawa, Y. Saito, *Carbon* **2012**, *50*, 1209 – 1215; b) K. Asaka, T. Nakayama, K. Miyazawa, Y. Saito, *Surf. Interface Anal.* **2012**, *44*, 780 – 783; c) K. Miyazawa, J. Minato, M. Fujino, T. Suga, *Diamond Relat. Mater.* **2006**, *15*, 1143 – 1146; d) K. Miyazawa, J. Minato, H. Zhou, T. Taguchi, I. Honma, T. Suga, *J. Eur. Ceram. Soc.* **2006**, *26*, 429 – 434.

[13] For comparison, we calcined resorcinol-formaldehyde colloidal polymer resin to prepare carbon under the identical conditions (2000 °C in vacuum), but the obtained surface area was quite low ($52\ m^2\ g^{-1}$).

[14] a) J. Minato, K. Miyazawa, *Carbon* **2005**, *43*, 2837 – 2841; b) J. Minato, K. Miyazawa, T. Suga, *Sci. Technol. Adv. Mater.* **2005**, *6*, 272 – 277; c) M. Rana, R. R. Bharathanatha, U. K. Gautam, *Carbon* **2014**, *74*, 44 – 53.

[15] a) H. Kuzmany, M. Matus, B. Burger, J. Winter, *Adv. Mater.* **1994**, *6*, 731 – 745; b) Z. Luo, X. Cheng, Y. Luo, B. H. Loo, A. Peng, J. Yao, *J. Am. Chem. Soc.* **2012**, *134*, 1130 – 1135.

[16] a) A. W. P. Fung, A. M. Rao, K. Kuriyama, M. S. Dresselhaus, M. Endo, N. Shindo, *J. Mater. Res.* **1993**, *8*, 489 – 500; b) N. Shimodaira, A. Masui, *J. Appl. Phys.* **2002**, *92*, 902 – 909; c) Y. Gogotsi, A. Nikitin, H. Ye, W. Zhou, J. E. Fischer, B. Yi, H. C. Foley, M. W. Barsoum, *Nat. Mater.* **2003**, *2*, 591 – 594; d) J. Zhao, L. Yang, F. Li, R. Yu, C. Jin, *Carbon* **2009**, *47*, 744 – 751.

[17] a) K. Ariga, Y. Yamauchi, Q. Ji, Y. Yonamine, J. P. Hill, *APL Mater.* **2014**, *2*, 030701 – 11; b) L. Jia, G. P. Mane, C. Anand, D. S. Dhawale, Q. Ji, K. Ariga, A. Vinu, *Chem. Commun.* **2012**, *48*, 9029 – 9031; c) J. Tang, N. L. Torad, R. R. Salunkhe, J. H. Yoon, M. S. A. Hossain, S. X. Dou, J. H. Kim, T. Kimura, Y. Yamauchi, *Chem. Asian J.* **2014**, *9*, 3238 – 3244.

